Nonlinear Dyn (2019) 98:1391–1402
https://doi.org/10.1007/s11071-019-05270-5

ORIGINAL PAPER

Traveling wave into an unstable state in dissipative oscillator chains

K. Alfaro-Bittner · M. G. Clerc · R. G. Rojas · M. A. García-Ñustes

Received: 1 February 2019 / Accepted: 21 September 2019 / Published online: 8 October 2019

Abstract Coupled oscillators can exhibit complex spatiotemporal dynamics. Here, we study the propagation of nonlinear waves into an unstable state in dissipative coupled oscillators. To this, we consider the dissipative Frenkel–Kontorova model, which accounts for a chain of coupled pendulums or Josephson junctions and coupling superconducting quantum interference devices. As a function of the dissipation parameter, the front that links the stable and unstable state is characterized by having a transition from monotonous to non-monotonous profile. In the conservative limit, these traveling nonlinear waves are unstable as a consequence of the energy released in the propagation. Traveling waves into unstable states are peculiar of dissipative coupling systems. When the coupling and the dissipation parameter are increased, the average front speed decreases. Based on an averaging method, we analytically determine the front speed. Numerical simulations show a quite fair agreement with the theoretical predictions. To show that our results are generic, we analyze a chain of coupled logistic equations. This model presents the predicted dynamics, opening the door to investigate a wider class of systems.

K. Alfaro-Bittner (✉) · R. G. Rojas · M. A. García-Ñustes
Instituto de Física, Pontificia Universidad Católica de Valparaíso, Casilla 4059, Valparaíso, Chile
e-mail: karin.alfaro.b@mail.pucv.cl

M. G. Clerc
Physics Department and Millennium Institute for Research in Optics, Facultad de Ciencias Físicas y Matemáticas, Universidad de Chile, Casilla 487-3, Santiago, Chile

Keywords Nonlinear wave · Front propagation · coupled oscillators

1 Introduction

Coupled oscillators are primordial to understanding the propagation of waves in continuous and discrete media [1]. An out-of-equilibrium coupled oscillators chain, that is coupled oscillators under the influence of injection and dissipation of energy, shows a variety of different phenomena [2–4] such as phase turbulence [2], synchronization [3], defects turbulence [5], random occurrence of coherence events [6], defect-mediated turbulence [7], spatiotemporal intermittency [8], quasiperiodicity in extended systems [9], chimera states [10,11], and particle-type solutions [12]. Depending on the nonlinearity, the oscillators may have more than one equilibrium, a phenomenon known as multistability. Due to the inherent fluctuations of macroscopic multistable systems, initial conditions, and physical imperfections, the system can develop different extended states or domains between the equilibria separated by walls [13]. These walls or interfaces are propagative because of the relative stability properties between the equilibria and curvature effects. Depending on the physical context, which can range from chemistry, biology to physics, the interfaces are known as front interfaces, domain walls, nonlinear waves, or wavefronts [13–20]. The propagation and dynamics of fronts depend on the nature of the states that are being connected. Fronts between stable

and unstable states have concentrated more research in the literature [20]. Pioneering studies in fronts propagation were performed in candle combustion by Faraday [17], gene propagation by Fisher [18], and population dynamics by Kolmogorov et al. [19]. In honor of these baseline studies, the fronts into unstable states are usually called *FKPP fronts* (see [20] and references therein). Initial conditions determine the speed and shape of these nonlinear waves. For bounded initial conditions, the FKPP front always propagates asymptotically with the minimum speed [21]. Experimentally, they have been observed in Taylor–Couette instability [22], Rayleigh–Benard convection [23], pearling and pinching on the propagating Rayleigh instability [24], spinodal decomposition in polymer mixtures [25], liquid crystal light valves with optical feedback [26,27], and population dynamics [14]. Recently, we have shown that front propagation into an unstable state in coupled dissipative nonlinear oscillators occurs in an oscillatory manner in the overdamped limit. Nevertheless, the front propagates in average with a distinctive speed that was determined analytically in the asymptotic limit [28].

The present manuscript aims to investigate the propagation of nonlinear waves into an unstable state in dissipative coupled oscillators. We consider a prototypical chain of oscillators, the dissipative Frenkel–Kontorova model. This model accounts for several physical systems such as the movement of atoms in condensed matter, magnetic chains, dynamics of coupled pendulums, and phase dynamics between superconductors (see the textbook [12] and references therein). As a function of the dissipation parameter, the FKPP front is characterized by having a transition from monotonous to non-monotonous profile. A monotonous nonlinear wave or front is characterized by a uniform increasing or decreasing profile between equilibria. In contrast, the profile of a non-monotonous front exhibits spatially damped oscillations toward the flank of the stable state.

In the conservative limit, wavefronts are unstable. Indeed, as a consequence of the released energy, the front core emits evanescent waves. Eventually, this radiation destabilizes the front solution. Hence, the front propagation into an unstable state is peculiar to dissipative coupled systems. Increasing the coupling and dissipation parameter, the average front speed decreases. Using an averaging method, we analytically determine the mean speed of the front. Numerical simulations show a quite fair agreement with the theoretical predictions. The observed front propagation is of a general nature and can be suitable for a wide class of systems. To extend our findings, we study a chain of logistic models, showing good accordance with predicted phenomena.

The paper has the following structure: The model of Frenkel–Kontorova is presented in Sect. 2. Likewise, the free energy, extended equilibria, different front solutions, and phase diagram of fronts of this system are characterized. The average front speed is characterized by numerically and analytically in Sect. 3. The propagation dynamics of the front is analyzed in Sect. 4. Due to the general nature of the observed dynamics, in Sect. 5, we consider a chain of logistic nonlinearity that exhibits the same type of phenomenology. Our conclusions and remarks are left to the final section.

2 The dissipative coupled oscillators model

2.1 The dissipative Frenkel–Kontorova model

Nonlinear oscillators such as the pendulum have played a primary role in understanding the complex dynamics [29–32]. Let us consider a dimensionless chain of dissipative coupled of pendulums,

$$\ddot{\theta}_i = \omega^2 \sin\theta_i - \mu\dot{\theta}_i + \kappa\left(\theta_{i+1} - 2\theta_i + \theta_{i-1}\right), \qquad (1)$$

where $\theta_i(t)$ is the angle formed by the pendulum and the vertical axis in the i-position at time t, $\theta_i = 0$ ($\theta_i = \pi$) corresponds to upside-down (upright) position of the pendulum (cf. Fig. 1a). Note that the origin of θ_i is not the usual. This election is used to make easier numerical and analytical calculations. All pendulums are identical, i indexes the i-th pendulum, ω is the natural frequency, μ accounts for the damping coefficient, and κ stands for the coupling strength. Let us introduce the distance dx between adjacent pendulums. Based on the continuous limit, this distance is related to the coupling strength by $\kappa = 1/dx^2$. This equation is also known as the Frenkel–Kontorova model. This model has been widely used to describe a chain of classical particles coupled to their nearest neighbors and under the effect of the on-site substrate potential in the context of crystal lattices. The model also appears in a variety of contexts as incommensurable phases in dielectrics materials, coupled identi-

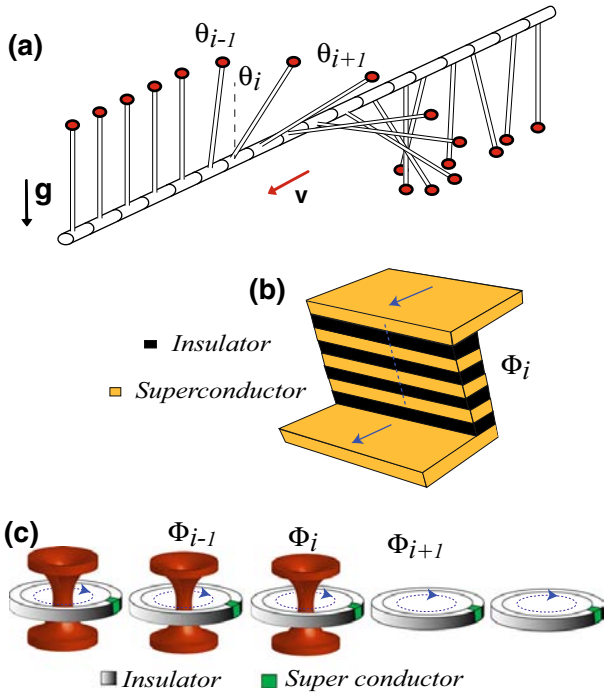

Fig. 1 Schematic representation of physical systems described by the dissipative Frenkel–Kontorova model. **a** A chain of dissipative coupled pendula. $\theta_i(t)$ is the angle formed by the pendulum and the vertical axis in the i-position at time t, $\theta_i = 0$ ($\theta_i = \pi$) corresponds to upside-down (upright) position of pendulum. **b** Coupling Josephson junctions. Φ_i accounts for the phase difference of adjacent superconductors. **c** Coupling superconducting quantum interference devices (SQUID), Φ_i accounts for the magnetic flux of i-th superconducting quantum device. The gray rings and green elements account for the insulators and superconductors, respectively. (Color figure online)

cal Josephson junctions, and coupling superconducting quantum interference devices (SQUIDS, see [12] and references therein).

Figure 1b and c shows schematic representations of a chain of coupled Josephson junctions and coupled SQUIDS. In these latter cases, Φ_i accounts, respectively, for the phase difference between the wave function of each superconductor in the i-th junction and the magnetic flux over i-th SQUIDS [33]. With the outbreak of new superconductor oscillators, to micrometer and nanometric scale, Josephson junction has acquired relevance [33]. These devices have played a fundamental role in detecting small magnetic fields in prospecting for mineral deposits, magnetoencephalography, and cosmic waves (see [34] and references therein). Hence, the deep understanding of the model Eq. (1) may allow having fresh applications in diverse physical contexts.

2.2 Front dynamics

The dynamics of dissipative coupled pendulums, Eq. 1, is characterized by minimizing the free energy

$$F[\theta_i, \dot{\theta}_i] \equiv \sum_{i=0}^{N} \left[\frac{\dot{\theta}_i^2}{2} + \omega^2 \cos\theta_i + \kappa \frac{(\theta_{i+1} - \theta_i)^2}{2} \right], \tag{2}$$

where the evolution is given by

$$\mu \dot{\theta}_i = -\frac{\delta F}{\delta \theta_i}. \tag{3}$$

The trivial equilibria of this extended system are the upside-down ($\theta_i = 0$, unstable state) and upright ($\theta_i = \pi$, stable state) position of pendulum. Recently, we have shown that this chain of coupled oscillators Eq. (1) in the overdamping limit ($\mu \sim O(1), \mu \geq 2$) has propagative solutions that connect these two equilibria [28]. This nonlinear wavefront was called π-kink. The physical origin of this propagation is that each time a pendulum decays from the unstable to the stable state kinetic energy releases. This energy is used by the pendulum chain as fuel for the front propagation. In this regime, the fronts are characterized by monotonously connecting the equilibria. Figure 2a shows the typical profile and spatiotemporal evolution of the front solution obtained from the numerical solutions of model, Eq. (1), with damping $\mu = 1.75$. All numerical simulations presented in the manuscript were done using finite differences method with Runge–Kutta order-4 algorithm. It is noteworthy that discrete coupled systems that exhibit bistability also present fronts between stable states [35].

To characterize the dynamics of the front, we introduce the auxiliary function $\theta(x, t)$ and the front position $P(t)$. $\theta(x, t)$ is the interpolation function of the angle in each oscillator $\theta_i(t)$. $P(t)$ denotes the front position such as $\theta(x = P, t) \equiv \pi/2$ which is fulfilled once starting from the unstable state. The point $P(t)$ does not necessarily correspond to an i-oscillator (a point on the grid). The vicinity of the front position $P(t)$ is known as the core of the front. Figure 2b and c shows the temporal evolution of the front position and speed for different strength of coupling κ between oscillators. From Fig. 2d, we infer that non-harmonic periodic oscillations characterize the front propagation in dissipative coupled oscillators as is reported in [28].

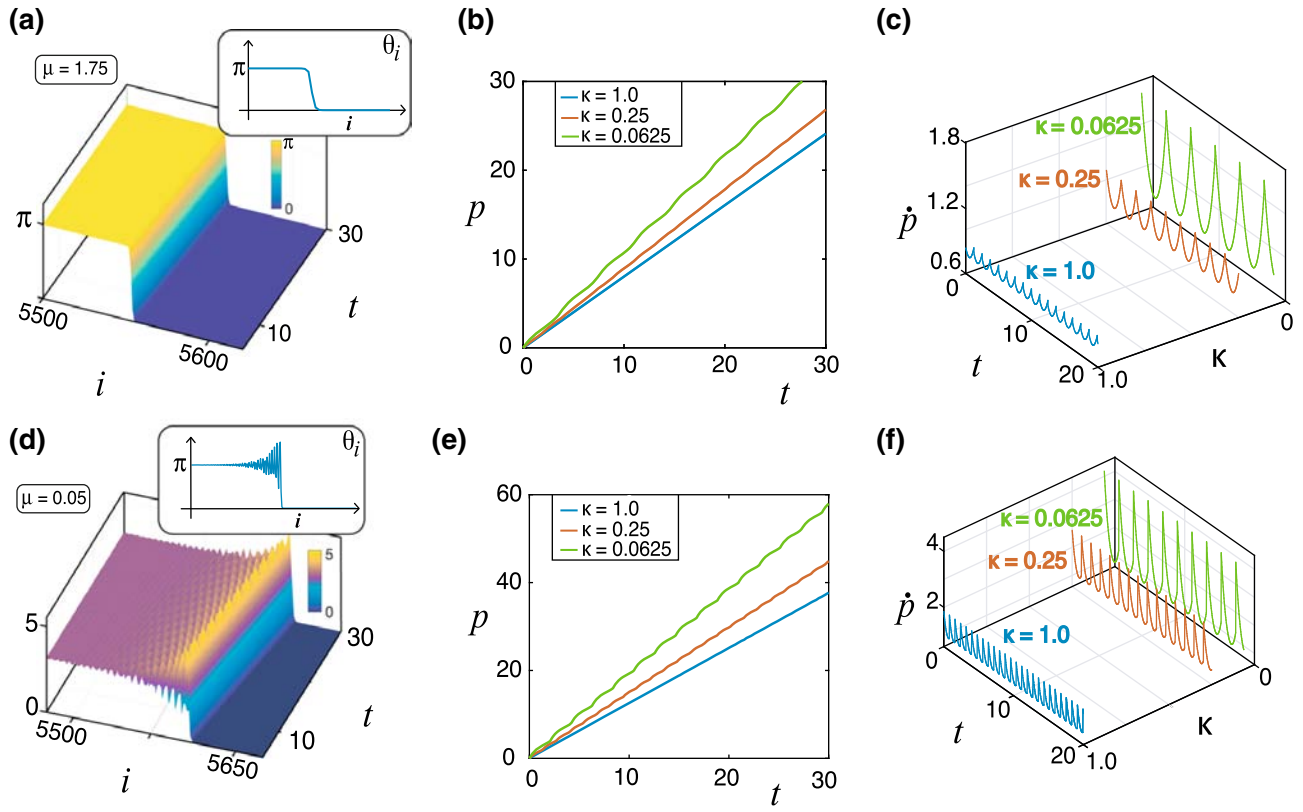

Fig. 2 Front solutions of the Frenkel–Kontorova model Eq. (1). Spatiotemporal evolution and profile of front solution with large (**a**) and small damping (**d**). Parameters are $\omega = 1.0, \kappa = 0.0625$, **a** $\mu = 1.75$, and **d** $\mu = 0.05$. Temporal evolution of the front position for different coupling strengths κ with large (**b**) and small damping (**e**). The speed of front position for different strengths of coupling between oscillators with large (**c**) and small damping (**f**). (Color figure online)

When the dissipation decreases, the previous scenario changes drastically. The front exhibits a bifurcation characterized by the emergence of spatially damped oscillations toward the flank of the stable state. Figure 2d displays the front spatiotemporal evolution and typical profile obtained from the numerical simulations of Eq. (1) with small damping $\mu \ll 1$. This type of spatial oscillations has been reported for a reaction–diffusion equation with inertia [36]. Experimentally, front propagation with spatially damping oscillations in intracellular calcium waves was observed [37]. Likewise, fronts between stable states exhibit the same type of transition [38]. The temporal evolution of the front position and speed for small values of the damping coefficient is alike as the dissipative case with $\mu \geq 2$. However, Fig. 2e and f reveals that the oscillating behavior increases in amplitude and frequency for $\mu \ll 1$.

Since it is a non-local bifurcation, the analytical study of the profile transition is a difficult task. However, numerically we are able to characterize the transition between monotonous and non-monotonous fronts. Figure 3 shows the bifurcation diagram as a function of the damping and the coupling strength parameter. For large dissipation, monotonous fronts are observed. When the dissipation decreases, non-monotonous fronts emerge. The Γ_1 curve accounts for the transition between these two types of fronts. This transition is supercritical. Indeed, when they appear, the spatially damped oscillations are characterized by having a small amplitude which increases as the dissipation decreases. By further decreasing the dissipation, fronts emit waves from their cores (see Fig. 4).

The emission of waves is because when the dissipation μ is reduced, it must release the energy by means of waves. Figure 4 shows a non-monotonous front with linear and nonlinear wave radiations. The waves close to the core are nonlinear and become linear as they travel away from it, (cf. Fig. 4). Further diminishing the dissipation, the nonlinear waves start to collide between

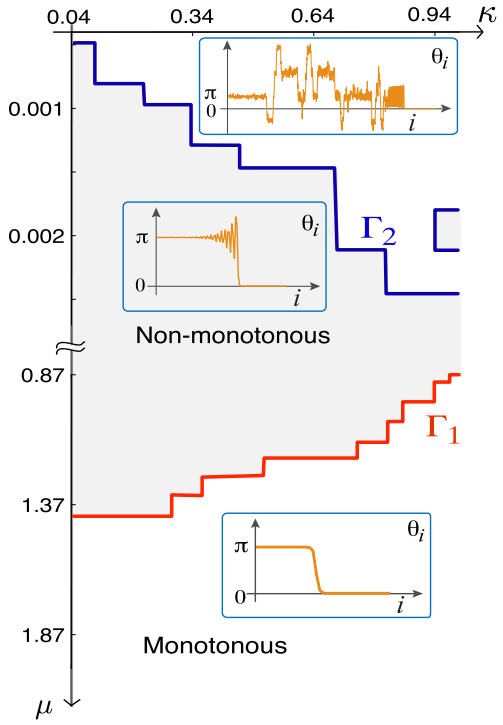

Fig. 3 Bifurcation diagram of fronts of model Eq. (1) by $\omega = 1$ in the space of the damping and the coupling strength parameter. The gray region shows where the non-monotonous fronts are observed. The lower region is characterized by exhibiting monotonous fronts. Γ_1 accounts for the transition curve between monotonous and non-monotonous fronts. The upper zone is a region where the fronts between upside-down and upright state are not persistent. In this zone, the fronts are observed as a transient dynamical behavior. Γ_2 is the separatrix curve between non-monotonous and not persistent fronts. The insets account for the typical fronts observed in the respective zones. (Color figure online)

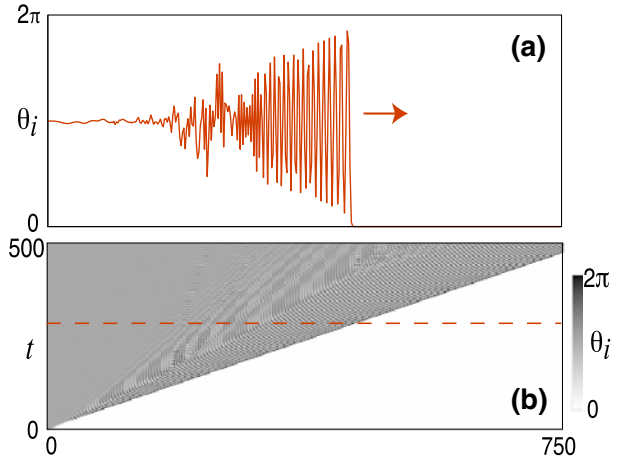

Fig. 4 Non-monotonous front solution of model Eq. (1) by $\omega = 1$, $\kappa = 1$, and $\mu = 0.002$. **a** Instantaneous profile of the front solution. **b** Spatiotemporal diagram of the non-monotonous front solution. (Color figure online)

them, generating localized waves of high amplitude, destabilizing the front solution. Figure 3 shows the transition curve Γ_2, between non-monotonous and non-persistent fronts. This curve was computed using the following criterion: If the front profile overcomes 2π, then the front is considered not persistent. A similar phenomenon has been reported in shock waves in the context of the discrete nonlinear Schrödinger equation with internal losses [39].

In brief, in the conservative limit ($\mu \to 0$), the traveling nonlinear waves connecting a uniform stable and unstable state are unstable, as a consequence of the energy released in the front propagation. Therefore, the front propagation into an unstable state is peculiar to dissipative coupled systems.

3 Characterization of front speed

The dissipative Frenkel–Kontorova equation (1) presents a traveling wave into an unstable state. These fronts are propagating with a non-harmonic oscillation speed. To characterize the front speed, let us introduce the average speed

$$\langle v \rangle = \frac{1}{T} \int_0^T \dot{P}(t) \mathrm{d}t, \tag{4}$$

where T is the oscillation period of the front speed. Numerically we have determined the period T and calculated the average front speed $\langle v \rangle$. Figure 5 shows the average front speed $\langle v \rangle$ as a function of the dissipation μ and the coupling strength κ. From this figure, we can infer that as the dissipation and intensity of coupling between oscillators increase, the average front speed decreases. Indeed, when the dissipation increases the system has less energy available to inject it to the front propagation. On the other hand, increasing the coupling is equivalent to interpreting that the distance between oscillators decreases since κ is inversely proportional to dx^2. Then, one expects the front speed to decrease.

3.1 Analytical determination of the average front speed

As we have mentioned, the initial conditions determine the front shape and the speed of propagation of a front into unstable states [20]. Localized disturbances

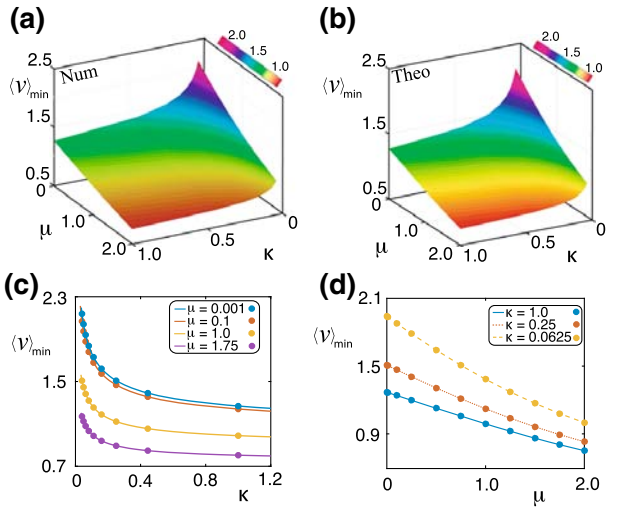

Fig. 5 Average front minimum speed $\langle v\rangle_{\min}$ as a function of the dissipation μ and the coupling strength κ of model Eq. (1) by $\omega = 1$. **a** Numerical and **b** analytical surface plot of the average front speed in the μ–κ parameters space. Analytical average front speed $\langle v\rangle_{\min}$ obtained from formulas (7) and (8) as a function of the dissipation μ and the coupling strength κ. **c** Minimal average front speed as a function of the coupling strength κ for different values of the dissipation. **d** $\langle v\rangle_{\min}$ as a function of μ for different values of κ. The points are obtained by numerical simulations of Eq. (1). The solid curves are obtained using formulas (7) and (8). (Color figure online)

are responsible, after a transient period, of the appearance of two counter-propagative fronts, which propagate with the minimum speed. Namely, any other disturbance at most can generate fronts that are spread faster or equal to the minimum speed. The determination of the minimum speed has attracted the attention of the scientific community since the dawn of the observation of fronts propagation. From the dynamical systems theory, the fronts correspond to homoclinic curves in the co-mobile system [20]. Hence, determining the front solution and its speed is a problem of non-local bifurcations. Unexpectedly, for systems with weakly nonlinear dynamics, the minimal front speed is ruled by the linear dynamics around the unstable state (marginal criterion) [19,20]. These types of nonlinear waves are called *pulled fronts*. Fronts, in which marginal criterium does not establish the minimal speed, are called *pushed fronts*. In the case of pushed fronts, the minimum speed is governed by the nonlinear terms (nonlinear criterion) [20]. A general characterization of the speed of pushed fronts is an open problem, and only in particular cases, there are analytical expressions. In the pioneering work of Kolmogorov et al. [19], they established when the marginal criterion governs the dynamics. Most precisely, they showed that the linear rate evolution around the unstable state, extended in the whole phase space, is greater than the dynamics of the system (weak nonlinearity).

To determine the front speed, we will use the strategy proposed in Ref. [28]. This strategy is based on proposing an ansatz for the profile of the front asymptotically around the unstable state. Because the front oscillates as it propagates, we consider the following ansatz for the front tail

$$\theta_i(t) = A\mathrm{e}^{(\alpha t - 2\beta i)}\left[1 + f^{\omega}_{\kappa;i}(t)\right], \tag{5}$$

where the amplitude A is a small constant that characterizes the shape of the front tail ($A \ll 1$), the index i is a positive and large integer number, $\alpha \equiv q\langle v\rangle$, $\beta \equiv q/2\sqrt{\kappa}$, and q are parameters. α and β account for the front speed and the rate of space decay, respectively. β is usually called steepness. ω is the frequency of front propagation. $f^{\omega}_{\kappa;i}(t)$ is a periodic function of frequency ω in the i-th position of the chain, which describes the oscillatory behavior of the propagation. Based on the observed dynamics in numerical simulations, we impose $f^{\omega}_{\kappa;i}(t) \to 0$ when $i/\sqrt{\kappa} \to \infty$. Introducing the above ansatz in Eq. (1) and taking into account only the linear leading terms, we obtain

$$\begin{aligned}\ddot{\theta}_i A^{-1}\mathrm{e}^{-(\alpha t-2\beta i)} &= \alpha^2\left[1 + f^{\omega}_{\kappa;i}\right] + 2\alpha\dot{f}^{\omega}_{\kappa;i} + \ddot{f}^{\omega}_{\kappa;i}\\ &= \omega^2\left[1 + f^{\omega}_{\kappa;i}\right] - \mu\left[\alpha\left[1 + f^{\omega}_{\kappa;i}\right]\right.\\ &\quad \left. + \dot{f}^{\omega}_{\kappa;i}(t)\right] + 4\kappa\sinh^2(\beta)\\ &\quad + \kappa\left(\mathrm{e}^{-2\beta}f^{\omega}_{\kappa;i+1} - 2f^{\omega}_{\kappa;i} + \mathrm{e}^{2\beta}f^{\omega}_{\kappa;i-1}\right).\end{aligned} \tag{6}$$

where we have divided by the factor $A^{-1}\mathrm{e}^{-(\alpha t-2i\beta)}$. Integrating this expression in a normalized period $T = 2\pi/\omega$ and using the fact that $\langle f^{\omega}_{\kappa;i}(t)\rangle = \langle \dot{f}^{\omega}_{\kappa;i}(t)\rangle = \langle \ddot{f}^{\omega}_{\kappa;i}(t)\rangle = 0$, after straightforward calculations and using the definition of α and q, we obtain

$$\langle v\rangle = -\frac{\mu}{4\beta\sqrt{\kappa}} + \frac{1}{2\beta\sqrt{\kappa}}\sqrt{\frac{\mu^2}{4} + \omega^2 + 4\kappa\sinh^2(\beta)}. \tag{7}$$

This formula stands for the average front speed as a function of the steepness β. Figure 6 displays the average front speed $\langle v\rangle$ as a function of the steepness β for different values of coupling strength κ. This average front speed is bounded from below by a minimum speed

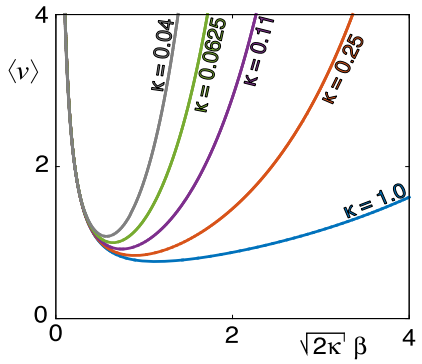

Fig. 6 Analytical front speed $\langle v\rangle$ as a function of the steepness β, obtained from formula (7) for different values of the coupling strength κ with $\mu = 2$. (Color figure online)

$\langle v\rangle_{\min}$. To derive the minimal mean front speed $\langle v\rangle_{\min}$, we differentiate the above speed with respect to β and imposing that is equal to zero, one gets

$$\omega^2\left(\frac{\mu^2}{4}+\omega^2\right)+16\kappa^2\sinh^2\beta_c\,[\sinh\beta_c-\beta_c\cosh\beta_c]^2 = 4\left[\left(\frac{\mu^2}{4}+\omega^2\right)\beta_c\sinh 2\beta_c-\left(\frac{\mu^2}{4}+2\omega^2\right)\sinh^2\beta_c\right]\kappa. \tag{8}$$

This expression gives us a relation between the critical steepness β_c and the coupling parameter κ. From Eq. (8), β_c is determined as a function of κ and μ [$\beta_c(\kappa,\mu)$], which has a complicated form. Using this expression in Eq. (7), we obtain $\langle v\rangle_{\min}(\kappa,\mu)$. Figure 5 shows $\langle v\rangle_{\min}$ as a function of κ and μ. Using expression (8) in formula (7), we obtain $\langle v\rangle_{\min}$ for the dissipative Frenkel–Kontorova model, Eq. 1. Note that this analytical result has a quite fair agreement with the numerical simulations as it is shown in Fig. 5. Therefore, this asymptotic procedure is a suitable method to characterize the mean properties of front propagation. Indeed, the marginal criterion determines the minimum average front speed of the dissipative Frenkel–Kontorova model, Eq. 1. It is important to note that the previous method is valid for monotonous or non-monotonous fronts since one only considers the asymptotic shape of the front toward the unstable state.

4 Waving dynamics of the front propagation

In the continuous limit, the fronts propagate as a rigid solid, that is, each front point moves with the same speed. Unexpectedly, when one considers coupled oscillators, different parts of the front propagate oscillating with the same frequency but with different amplitudes [28], describing a *waving dynamics*. To characterize this waving dynamics, we study the dynamics of two additional front points $P_u(t)$ and $P_d(t)$ located above and below of $P(t)$, where $\theta(x = P_u, t) \equiv \theta_u$ and $\theta(x = P_d, t) \equiv \theta_d$ are fulfilled once starting from the unstable state, with θ_u and θ_d given arbitrarily. Figure 7a shows the temporal evolution of $P_u(t)$, $P_d(t)$ and $P(t)$. Note that they oscillate in out of phase and with the same frequency. The amplitudes of oscillation are different depending on the position. In contrast, the non-monotonous front displays a different configuration. The oscillations are in phase and with the same frequency, see Fig. 7b.

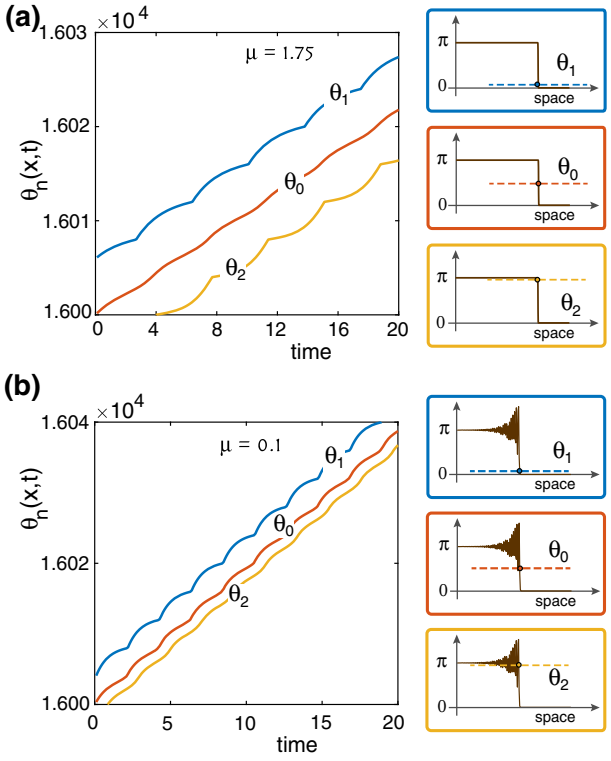

Fig. 7 Waving dynamics of the front propagation of the dissipative Frenkel–Kontorova equation (1) by $\omega = 1$ and $\kappa = 0.0625$. Temporal evolution of different points of the monotonous (**a**) and the non-monotonous (**b**) fronts. The right panels show the profile of the front at a given time and illustrate the values of the front $\theta_u = 9\pi/10$, $\theta_p = \pi/2$, and $\theta_d = \pi/5$ considered to determine the positions P_u, P, and P_d. (Color figure online)

Figure 8a illustrates the spatiotemporal evolution of the front. We can notice that most of the waving dynamical behavior occurs around the front core. Figure 8b indicates the amplitude of different points on the front. This waving dynamic behavior is observed for monotonous and non-monotonous fronts.

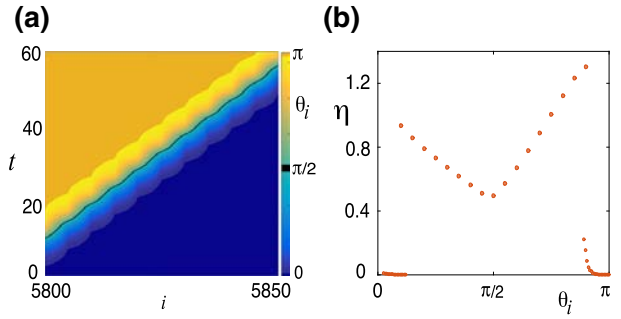

Fig. 8 Waving dynamics on front propagation in the dissipative Frenkel–Kontorova equation (1) by $\omega = 1$, $\mu = 2$, and $\kappa = 0.04$. **a** Spatiotemporal evolution. **b** Oscillation amplitude η of different front points. (Color figure online)

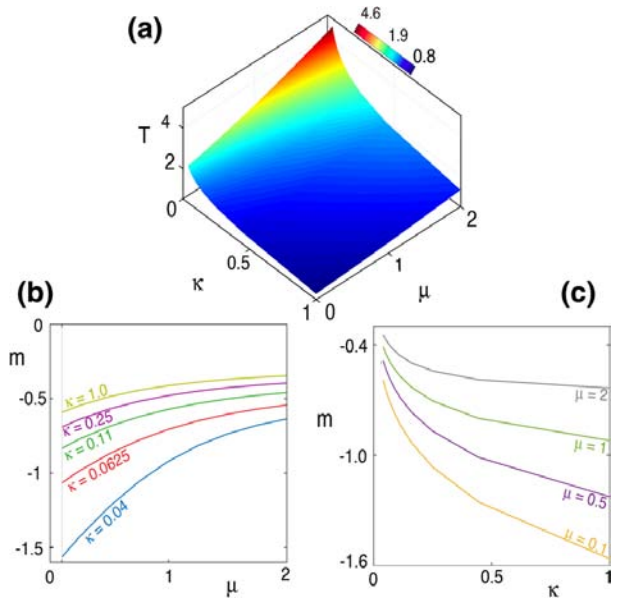

Fig. 9 Characterization of the dynamics of the front position of model Eq. (1) with $\omega = 1$. **a** Surface plot of the period of front position $T(\kappa, \mu)$ as a function of κ–μ space. **b** Slope of the front position as a function of the dissipation μ for different values of coupling strength κ. **c** Slope of the front position as a function coupling strength κ for different values of the dissipation μ. (Color figure online)

From the evolution of the front position, one can characterize its period T and its slope m. As the coupling strength κ increases, the period T decreases. This is due to the nucleation barrier of the Peierls–Nabarro potential increasing with κ [12,28]. On the contrary, as the dissipation μ increases, the period increases. Indeed, as the dissipation grows, the system has less available energy. Thus, the oscillation decreases in frequency. These results are summarized in Fig. 9a.

Similarly, we characterize the slope of the front position m as a function of κ and μ. Figure 9b and c shows the slope of the front position on κ–μ space. Around $\mu \sim 10^{-2}$, the non-monotonous front starts to destabilize, hindering an appropriate characterization of the slope for smaller values of μ. The vertical dashed line in Fig. 9b indicates qualitatively the limit. For larger values of μ, the slope is well defined and it increases with μ and decreases with κ (Fig. 9b and c). Based on the result of Ref. [40], we provide a qualitative explanation. In the continuous limit, the slope m is related to the front speed $\langle v \rangle$ [40]. From expression (7) it is observed that the slope grows as a function of μ, following a square root function and saturating to a given value, proportional to coupling κ. On the other hand, for κ close to zero, the slope of the front must grow exponentially. While for an increasing κ, it must decrease. Figure 9b and c shows a good agreement between this interpretation and numerical measurements.

5 Robust dynamics in dissipative coupling chains

The dynamics presented in the previous sections must be generic when is considered multistable coupled systems. A minimal model that contains the above ingredients is a dissipative coupling system with logistic nonlinearity, which reads

$$\ddot{u}_i + \mu \dot{u}_i = u_i(1 - u_i) + \kappa(u_{i+1} - 2u_i + u_{i-1}), \quad (9)$$

where u_i is an order parameter that describes, for example, the dynamics around a transcritical instability [41], μ is the damping coefficient, and κ accounts for the coupling strength. Models with nonlinear logistic have been used to describe the dynamics of populations in ecology, chemical reactions, among others.

The model Eq. (9) has two equilibria $u_i = 0$ and $u_i = 1$, which are unstable and stable states, respectively. Hence, one expects to observe nonlinear traveling wave solutions between these equilibria. Figure 10 shows front solutions exhibited by Eq. (9). For small and large dissipation, monotonous and non-monotonous fronts are observed. Their oscillatory nature characterizes the propagation of these fronts. As a function of the dissipation and the coupling strength, the front speed exhibits similar behavior to those presented by the Frenkel–Kontorova model Eq. (1). Therefore, the dynamics of fronts presented by these coupling systems is generic and is not particular to the models considered.

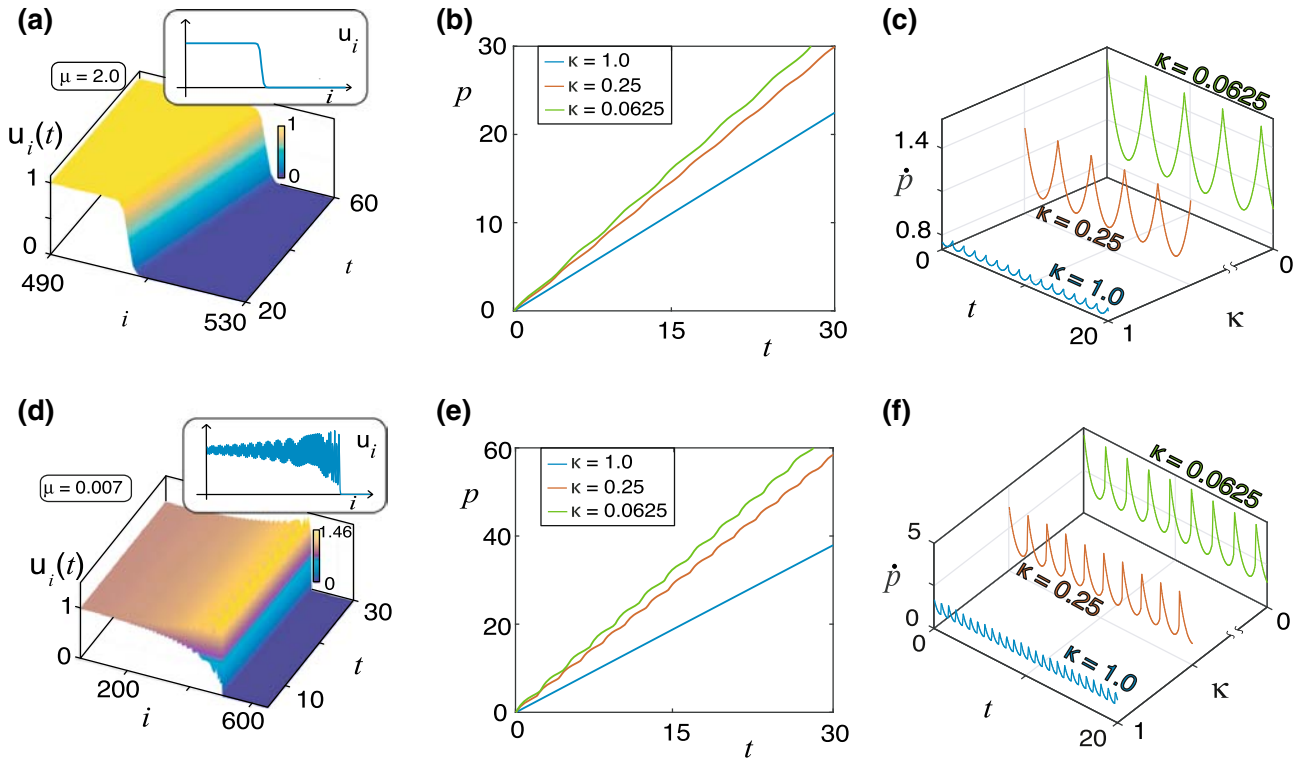

Fig. 10 Nonlinear traveling wave solutions of a chain with logistics nonlinearity model Eq. (9). Spatiotemporal evolution and profile of front solution $u_i(t)$ with small and large damping, and $\kappa = 0.0625$, **a** $\mu = 2.0$, and **d** $\mu = 0.007$. Temporal evolution of the front position for different coupling strengths κ with large (**b**) and small damping (**e**). The speed of front position for different values of the coupling strength with large (**c**) and small damping (**f**). (Color figure online)

5.1 Analytical characterization of the front speed

To understand more deeply the propagation of fronts, we can consider the overdamped limit (large dissipation, $\mu \gg 1$) of model Eq. (9). Namely, one can neglect the inertia of model Eq. (9) and renormalize the timescale. In this limit, analytical calculations can be made and compared with the numerical observations. Using the same strategy used in Sect. 3 to determine the front speed, we use the ansatz

$$u_i(t) = U\mathrm{e}^{(\alpha t - 2\beta i)}\left[1 + f^{\omega}_{\kappa;i}(t)\right], \qquad i \gg 1, \quad (10)$$

where U is a small constant that characterizes the shape of the front tail ($U \ll 1$), $\alpha \equiv q\langle v\rangle$, and $\beta \equiv q/2\sqrt{\kappa}$, respectively, account for the front speed and the steepness, ω is the frequency of front propagation, and $f^{\omega}_{\kappa;i}(t)$ is a periodic function of frequency ω in the i-th position of the chain.

Introducing the above ansatz (10) in Eq. (9), considering the linear leading terms in U, and averaging in a period of the front propagation, after straightforward calculations, we get

$$\langle v\rangle = \frac{1}{2\sqrt{\kappa}\beta} + 2\sqrt{\kappa}\beta\left(\frac{\sinh\beta}{\beta}\right)^2. \quad (11)$$

Note that expression (11) can be obtained alternatively from Eq. (7) in the overdamped limit $\mu \gg 1$ and rescaling time.

The front speed as a function of the steepness is also bounded by below, that is, there is a single minimum front speed. Figure 11 illustrates the front speed $\langle v\rangle$ as a function of the steepness $2\sqrt{\kappa}\beta$. In the limit that $2\sqrt{\kappa}\beta$ tends to zero, one can recover the standard formula $\langle v\rangle = 1/2\sqrt{\kappa}\beta + 2\sqrt{\kappa}\beta$ [42].

To minimize the average front speed, we differentiate the above speed Eq. (11) with respect to β and imposing that is equal to zero, one gets

$$\kappa^{-1} = 4\sinh\beta_c(2\beta_c\cosh\beta_c - \sinh\beta_c), \quad (12)$$

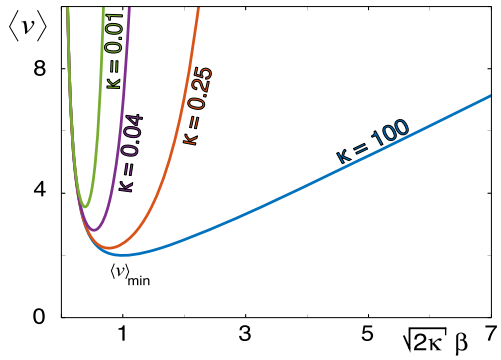

Fig. 11 Analytical front speed $\langle v \rangle$ as function of the steepness β, obtained from formula (11) for different values of the coupling strength κ. (Color figure online)

where $\beta_c(\kappa)$ stands for the steepness of the front with a minimal speed. Using a similar analysis performed for the Frenkel–Kontorova model Eq. (1), the minimum average speed is obtained using expression (12) in formula (11). However, this expression is an implicit elaborated formula of the coupling strength κ. In the case that the strength is large enough, $\kappa \gg 1$ ($\beta_c \ll 1$), we can use the expression

$$\kappa \approx 1/4\beta_c^2(1+\beta_c^2). \tag{13}$$

Figure 12a shows a comparison between numerical measurements, analytical results, and formula (13). For large coupling strength, the above approximation adequately describes the front propagation (see Fig. 12a). Using expression (13), one can find the following minimum averaged front speed

$$\langle v \rangle_{\min} \approx v_0 \left[1 + 4\kappa \sinh^2 \left(\frac{1}{\sqrt{2\kappa^{-1}\left(1+\sqrt{1+\kappa^{-1}}\right)}} \right) \right], \tag{14}$$

where $v_0 \equiv \sqrt{1+\sqrt{1+\kappa^{-1}}/2}$. Figure 12b shows $\langle v \rangle_{\min}$ as a function of the coupling strength κ and a comparison between numerical and analytical results. Numerical and analytical results present an excellent agreement. For large coupling strength, approach (14) adequately accounts for the front propagation (see Fig. 12b). Note that the overdamping limit of the dissipative Frenkel–Kontorova model can be used with the same strategy to determine the minimum speed of Eq. (9).

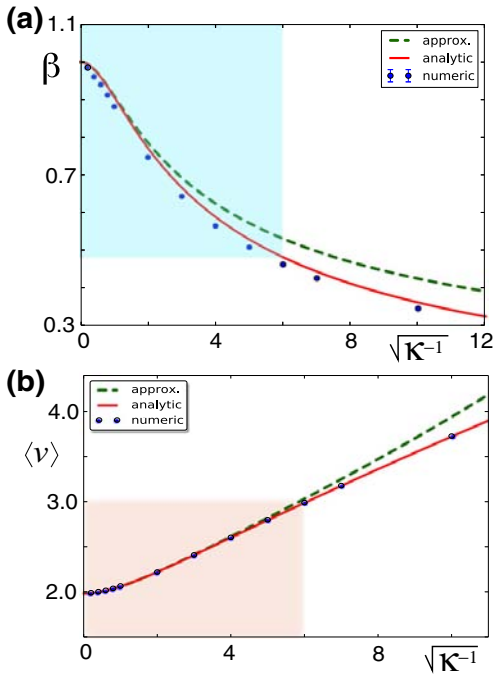

Fig. 12 Minimal average front speed of the chain with logistics nonlinearity model Eq. (9). **a** Steepness β as a function of the square root of the coupling strength κ, obtained from formula (12). Points are obtained by numerical simulations of model Eq. (9) by $\mu = 1$. The continuous and dashed curves are obtained using formulas (12) and (13), respectively. **b** Minimal average front speed as a function of the square root of the coupling strength κ. Points are obtained by numerical simulations of model Eq. (9) by $\mu = 1$. The continuous curve is acquired using formulas (11) and (12). The dashed curve is obtained by considered formula (14). The painted area emphasizes the region where the approach (12) adequately describes the front propagation. (Color figure online)

6 Conclusions and remarks

Dissipative nonlinear coupled oscillators can exhibit coexistence of different extended states. Small and localized perturbations of a steady state are characterized by exhibiting dispersive damped waves. This scenario changes drastically when one disturbs an extended unstable state. Due to the constant release of energy, if the dissipation is large enough, two nonlinear counter-propagating waves are observed [43]. These waves propagate from a stable state into an unstable one. We have investigated this phenomenon considering a prototypical chain of oscillators, the dissipative Frenkel–Kontorova model. We have characterized a traveling wave solution as a function of the dissipation and coupling strength parameter. These nonlinear waves have a transition from monotonous

to non-monotonous profile. A monotonous and non-monotonous profile has been observed experimentally in several dissipative systems [20] and intracellular calcium waves [37], respectively. We have revealed the phase diagram of traveling nonlinear waves. In the conservative limit, the front solutions are unstable, as a consequence of the energy released in the front propagation. This instability is driven by the interaction of localized nonlinear waves. Therefore, the front propagation into an unstable state is a peculiar phenomenon of dissipative coupling systems. Due to the discrete nature of coupling systems, the front propagation presents a waving dynamics. When the coupling and dissipation parameters increase, the average front speed decreases. Using the averaging method, we have analytically determined the average front speed. Numerical simulations show a quite fair agreement with the theoretical predictions. The studied dynamics of front propagation can be observed in a wide class of systems as a chain of logistic models. Besides, the methodology presented is suitable for other physical systems. The chain of logistic model presents the same dynamics observed in the Frenkel–Kontorova chain [28].

SQUIDS opens the possibility of considering new configurations of coupled oscillators and fresh applications in the detection of small magnetic fields. The characterization of traveling waves in coupled oscillators in two dimensions is an unsolved problem. A study in this direction is in progress.

Acknowledgements M.G.C. thanks for the financial support of Millenium Institute for Research in Optics (MIRO). M.A.G-N. and R.G.R thank for the financial support of Proyecto Interno Regular Pontificia Universidad Católica de Valparaíso Nos. 039.306/2018 and 039.007/2018, respectively. K.A-B acknowledges the financial support of Comisión Nacional de Investigación Científica y Tecnológica (CONICYT) by Doctorado Nacional 2014-No. 21140668.

Compliance with ethical standards

Conflict of interest The authors declare that they have no conflict of interest.

References

1. Fetter, A.L., Walecka, J.D.: Theoretical Mechanics of Particles and Continua. Dover Publications, New York (2003)
2. Kuramoto, Y.: Chemical Oscillations, Waves, and Turbulence. Springer, Berlin (1984)
3. Pikovsky, A., Rosenblum, M., Kurths, J., Hilborn, R.C.: Synchronization: A Universal Concept in Nonlinear Sciences. Cambridge University Press, Cambridge (2002)
4. Kaneko, K., Tsuda, I.: Chaos and Beyond: A Constructive Approach with Applications in Life Sciences. Springer, Berlin (1996)
5. Shraiman, B.I., Pumir, A., van Saarloos, W., Hohenberg, P.C., Chate, H., Holen, M.: Spatiotemporal chaos in the one-dimensional complex Ginzburg–Landau equation. Physica D **57**, 241–248 (1992)
6. Newell, A.C., Rand, D.A., Russell, D.: Turbulent transport and the random occurrence of coherent events. Physica D Nonlinear Phenom. **33**, 281–303 (1988)
7. Coullet, P., Gil, L., Lega, J.: Defect-mediated turbulence. Phys. Rev. Lett. **62**, 1619–1622 (1989)
8. Chate, H.: Spatiotemporal intermittency regimes of the one-dimensional complex Ginzburg–Landau equation. Nonlinearity **7**, 185–204 (1999)
9. Clerc, M.G., Verschueren, N.: Quasiperiodicity route to spatiotemporal chaos in one-dimensional pattern-forming systems. Phys. Rev. E **88**, 052916 (2013)
10. Clerc, M.G., Coulibaly, S., Ferré, M.A., García-?ustes, M.A., Rojas, R.G.: Chimera-type states induced by local coupling. Phys. Rev. E **93**, 052204 (2016)
11. Clerc, M.G., Coulibaly, S., Ferré, M.A., Rojas, R.G.: Chimera states in a Duffing oscillators chain coupled to nearest neighbors. Chaos **28**, 083126 (2018)
12. Braun, O.M., Kivshar, Y.S.: The Frenkel–Kontorova Model: Concepts, Methods, and Applications. Springer, Berlin (2013)
13. Pismen, L.M.: Patterns and Interfaces in Dissipative Dynamics. Springer, Berlin (2006)
14. Murray, J.D.: Mathematical Biology I and II. Springer, New York (2001)
15. Cross, M., Greenside, H.: Pattern Formation and Dynamics in Nonequilibrium Systems. Cambridge University Press, New York (2009)
16. Langer, J.S.: Instabilities and pattern formation in crystal growth. Rev. Mod. Phys. **52**, 1 (1980)
17. Faraday, M.: Course of Six Lectures on the Chemical History of a Candle. Griffin, Bohn & Co, London (1861)
18. Fisher, R.A.: The wave of advance of advantageous genes. Ann. Eugen. **7**, 355–369 (1937)
19. Kolmogorov, A., Petrovsky, I., Piscounov, N.: Study of the diffusion equation with growth of the quantity of matter and its application to a biology problem. Bull. Univ. Mosc. Ser. Int. A **1**, 1–26 (1937)
20. Van Saarloos, W.: Front propagation into unstable states. Phys. Rep. **386**, 29–222 (2003)
21. Aronson, D.G., Weinberger, H.F.: Multidimensional nonlinear diffusion arising in population dynamics. Adv. Math. **30**, 33 (1978)
22. Ahlers, G., Cannell, D.S.: Vortex-front propagation in rotating Couette–Taylor flow. Phys. Rev. Lett. **50**, 1583 (1983)
23. Fineberg, J., Steinberg, V.: Vortex-front propagation in Rayleigh–Bénard convection. Phys. Rev. Lett. **58**, 1332 (1987)
24. Powers, T.R., Goldstein, R.E.: Pearling and pinching: propagation of Rayleigh instabilities. Phys. Rev. Lett. **78**, 2555 (1997)

25. Langer, J.: An introduction to the kinetics of first-order phase transition. In: Godrèche, C. (ed.) Solids Far from Equilibrium. Cambridge University Press, Cambridge (1992)
26. Clerc, M.G., Nagaya, T., Petrossian, A., Residori, S., Riera, C.S.: First-order Fréedericksz transition and front propagation in a liquid crystal light valve with feedback. Eur. Phys. J. D **28**, 435 (2004)
27. Alfaro-Bittner, K., Castillo-Pinto, C., Clerc, M.G., González-Cortés, G., Rojas, R.G., Wilson, M.: Front propagation into an unstable state in a forced medium: experiments and theory. Phys. Rev. E **98**, 050201 (2018)
28. Alfaro-Bittner, K., Clerc, M.G., García-Ñustes, M.A., Rojas, R.G.: π-kink propagation in the damped Frenkel–Kontorova model. EPL **119**, 40003 (2017)
29. Benson, T.: Principles of Vibration. Oxford University Press, Oxford (2001)
30. Karnopp, D.: Computer simulation of stick-slip friction in mechanical dynamic systems. J. Dyn. Sys. Meas. Control **107**, 100–103 (1985)
31. Den Hartog, J.P.: Mechanical Vibrations. Dover publications, New York (1985)
32. Baker, G.L., Blackburn, J.A.: The Pendulum: A Case Study in Physics. Oxford University Press, New York (2005)
33. Likharev, K.K.: Dynamics of Josephson Junctions and Circuits. Gordon and Breach science publishers, New York (1985)
34. Clarke, J., Braginski, A.I.: The SQUID Handbook: Applications of SQUIDs and SQUID Systems. Wiley, Hoboken (2006)
35. Clerc, M.G., Elías, R.G., Rojas, R.G.: Continuous description of lattice discreteness effects in front propagation. Philos. Trans. R. Soc. A **369**, 412 (2011)
36. Manne, K.K., Hurd, A.J., Kenkre, V.M.: Nonlinear waves in reaction-diffusion systems: the effect of transport memory. Phys. Rev. E **61**, 4177 (2000)
37. Ponce, S., Keizer, J., Pearson, J.E.: Fire-diffuse-fire model of dynamics of intracellular calcium waves. Proc. Natl. Acad. Sci. USA **96**, 6060 (1999)
38. Clerc, M.G., Escaff, D., Kenkre, V.M.: Patterns and localized structures in population dynamics. Phys. Rev. E **72**, 056217 (2005)
39. Salerno, M., Malomed, B.A., Konotop, V.V.: Shock wave dynamics in a discrete nonlinear Schrödinger equation with internal losses. Phys. Rev. E **62**, 8651 (2000)
40. Aronson, D.G., Weinberger, H.F.: Nonlinear diffusion in population genetics, combustion, and nerve pulse propagation. In: Goldstein, J.A. (ed.) Partial Differential Equations and Related Topics. Springer, Berlin Heidelberg, Berlin (1975)
41. Strogatz, S.H.: Nonlinear Dynamics and Chaos: With Applications to Physics, Biology, Chemistry, and Engineering. CRC Press, Boca Raton (2018)
42. Mollison, D.: Spatial contact models for ecological and epidemic spread. J. R. Stat. Soc. B **39**, 283 (1977)
43. Andrade-Silva, I., Clerc, M.G., Odent, V.: Asymmetric counterpropagating fronts without flow. Phys. Rev. E **91**, 060501 (2015)